Self-assembly, nematic phase formation and organocatalytic behaviour of a proline-functionalized lipopeptide

Pelin, J. N. B. D., Edwards-Gayle, C. J. C., Castelletto, V., Aguilar, A. M., Alves, W. A., Seitsonen, J., Ruokolainen, J. and Hamley, I. W. (2020) Self-assembly, nematic phase formation and organocatalytic behaviour of a proline-functionalized lipopeptide. ACS Applied Materials & Interfaces, 12 (12). pp. 13671-13679. ISSN 1944-8252 doi: https://doi.org/10.1021/acsami.0c00686 Available at https://centaur.reading.ac.uk/89358/

ACS APPLIED MATERIALS & INTERFACES

www.acsami.org

Research Article

Self-Assembly, Nematic Phase Formation, and Organocatalytic Behavior of a Proline-Functionalized Lipopeptide

Juliane N.B.D. Pelin, Charlotte J. C. Edwards-Gayle, Valeria Castelletto, Andrea M. Aguilar, Wendel A. Alves, Jani Seitsonen, Janne Ruokolainen, and Ian W. Hamley*

Cite This: https://dx.doi.org/10.1021/acsami.0c00686

Read Online

ACCESS | Metrics & More | Article Recommendations | Supporting Information

ABSTRACT: The self-assembly of the amphiphilic lipopeptide PAEPKI-C_{16} (P = proline, A = alanine, E = glutamic acid, K = lysine, I = isoleucine, and C_{16} = hexadecyl) was investigated using a combination of microscopy, spectroscopy, and scattering methods and compared to that of C_{16}-IKPEAP with the same (reversed) peptide sequence and the alkyl chain positioned at the N-terminus and lacking a free N-terminal proline residue. The catalytic activity of these peptides was then compared using a model aldol reaction system. For PAEPKI-C_{16}, the cryo-TEM images showed the formation of micrometer-length fibers, which by small-angle X-ray scattering (SAXS) were found to have radii of 2.5−2.6 nm. Spectroscopic analysis shows that these fibers are built from β-sheets. This behavior is in complete contrast to that of C_{16}-IKPEAP, which forms spherical micelles with peptides in a disordered conformation [Hutchinson et al. *J. Phys. Chem. B* **2019**, *123*, 613]. In PAEPKI-C_{16}, spontaneous alignment of fibers was observed upon increasing pH, which was accompanied by observed birefringence and anisotropy of SAXS patterns. This shows the ability to form a nematic phase, and unprecedented nematic hydrogel formation was also observed for these lipopeptides at sufficiently high concentrations. SAXS shows retention of an ultrafine (1.7 nm core radius) fibrillar network within the hydrogel. PAEPKI-C_{16} with free N-terminal proline shows enhanced *anti:syn* diastereoselectivity and better conversion compared to C_{16}-IKPEAP. The cytotoxicity of PAEPKI-C_{16} was also lower than that of C_{16}-IKPEAP for both fibroblast and cancer cell lines. These results highlight the sensitivity of lipopeptide properties to the presence of a free proline residue. The spontaneous nematic phase formation by PAEPKI-C_{16} points to the high anisotropy of its ultrafine fibrillar structure, and the formation of such a phase at low concentrations in aqueous solution may be valuable for future applications.

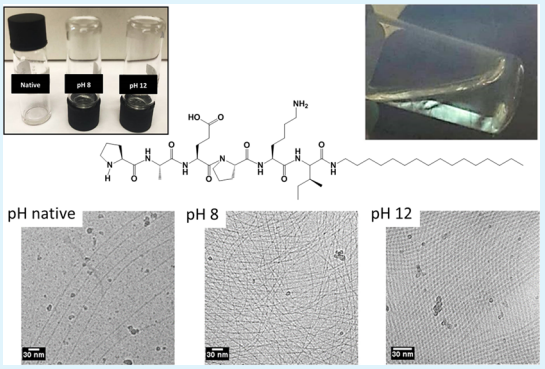

KEYWORDS: *lipopeptides, self-assembly, fibers, hydrogel, nematic, biocatalysis*

INTRODUCTION

Organocatalysts incorporating L-proline residues have been employed in asymmetric catalysis for a wide range of synthetic reactions.[1] Proline-based organocatalysts containing long hydrophobic chains have been found to catalyze aldol reactions in reaction mixtures containing both water and organic solvents.[2] A lipidated peptide with a C_{16} (hexadecyl, palmitoyl) chain attached at the C-terminus and a proline-based head group (PRW-C_{16}) was found to have high catalytic activity for aldol reactions performed in water, with very good stereoselectivity and conversion rates.[3] The lipidated peptide self-assembles in the form of spherical micelles above a critical aggregation concentration (cac), and the self-assembled structures are responsible for catalytic properties, since poor results were obtained in the absence of lipidated assembles. In another example, Escuder et al. studied aldol reactions catalyzed by L-proline-derived peptides that form organogels[4] or hydrogels.[5]

Aldol reactions combine two carbonyl compounds to form a new C−C bond, to produce a compound containing a β-hydroxy carbonyl group,[6,7] which is found in living organisms and has exceptional pharmacological activities. Since the 1970s, it has been known that L-proline is a very efficient organocatalyst for aldol reactions.[8] Many aldol reactions involving L-proline are performed in organic solvents such as dimethyl sulfoxide (DMSO) and chloroform, which are harmful and environmentally unfavorable.[3] As a result, there is a current drive to overcome this by replacing these solvents with green solvents such as water. The use of water is also attractive for promoting self-assembly via hydrophobic

Received: January 13, 2020
Accepted: March 5, 2020
Published: March 5, 2020

Scheme 1. Molecular Structures of (Top) PAEPKI-C_{16} and (Bottom) C_{16}-IKPEAP

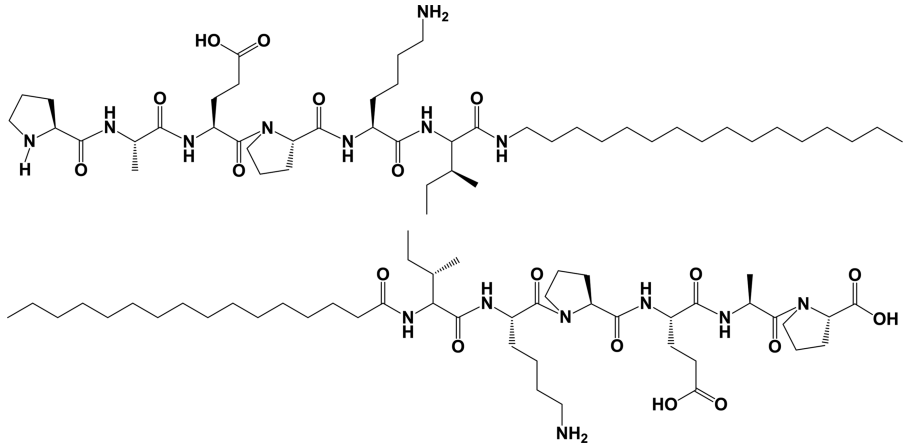

interactions and hydrogen bonding. Lipidation of peptides commonly leads to self-assembly in aqueous solution into a variety of nanostructures including micelles, nanotapes, and nanofibrils.[9−12] Lipopeptides are a type of peptide amphiphile (PA).

Recently, our group studied the effect of the substitution of an ester with an amide linkage between the hydrophobic lipid chain and the hydrated peptide head group in the PRW-C_{16} lipopeptide.[13] The linker group may influence the biocatalytic activity because of differences in the local conformation around the catalytic site and/or the polarization of the amide or ester linkages. Aldol reactions using cyclohexanone and *p*-nitrobenzaldehyde showed that PRW-NH-C_{16} has a high enantiomeric excess (88−89%) and diastereoselectivity (93:7 *anti*:*syn*) compared to PRW-O-C_{16} (71−84%, 91:9). Both lipopeptides self-assemble into spherical micelles. However, the spherical micelles formed by PRW-NH-C_{16} are slightly larger than those of PRW-O-C_{16}, and this along with the configuration of the tripeptide micellar corona leads to a higher conversion.

Peptide hormones are attracting interest as targets for novel therapeutics and diagnostics. Some of us have recently been investigating the self-assembly of derivatives of the human gut hormone PYY_{3-36}, which is one of the pancreatic peptides and is a therapeutic target for obesity since it is a signal of satiety following food intake.[14−17] The self-assembly of lipidated and PEGylated analogues, which were designed to have enhanced stability and circulation time, was investigated. Lipidated PYY_{3-36} peptides can form spherical micelles or fibrils depending on the nature of the lipid chain and the solution pH.[18,19] The PEGylated PYY_{3-36} variants studied formed irregular aggregates.[19]

Fragment peptides may retain significant activity of the parent full-sequence peptide but with improved ease of synthesis and cost-effectiveness. We therefore examined lipopeptides containing PYY_{3-36} fragments. We recently studied the self-assembly of C_{16}-IKPEAP and C_{16}-IKPEAPGE, which contain N-terminal hexameric and octameric sequences from PYY_{3-36}.[20] Both these lipopeptides form spherical micelles that are stable over a wide pH range, above defined critical aggregation concentrations. Circular dichroism (CD) spectroscopy showed that the lipidated peptides have disordered structures, in contrast to the polyproline II (PPII) conformation of the peptides themselves. Notably, upon drying these samples, β-sheet fibrillar ("amyloid-like") fibrils are observed.[20]

Here, we study a related variant of PYY_{3-36}, with a palmitoyl chain (hexadecyl, C_{16}) attached to the peptide head group at the C-terminus. The peptide sequence is PAEPKI (Scheme 1), which is the reverse of IKPEAP, the C-terminal hexapeptide from PYY_{3-36}.

As shown in Scheme 1, PAEPKI-C_{16} differs from C_{16}-IKPEAP for two reasons: first, the P residue is free at the N terminus (unlike C-terminal P-COOH in C_{16}-IKPEAP), and second, the palmitoyl chain is attached C terminally via CONH rather than via the NHCO-$C_{15}H_{31}$ N-terminal linkage in C_{16}-IKPEAP.

PAEPKI-C_{16} was synthesized to have a free terminal P residue in order to study its activity as a proline-based organocatalyst of a model aldol reaction. Results from this investigation are presented herein. In addition, we examine the self-assembly of the lipopeptide by first determining the cac using fluorescence probe assays. The conformation of the peptide is then studied using CD spectroscopy and X-ray diffraction, and the self-assembled structure is determined using small-angle X-ray scattering. The results are compared to those previously reported for C_{16}-IKPEAP.[20] We unexpectedly found that at a sufficiently high concentration, PAEPKI-C_{16} spontaneously forms a nematic phase in water, and this lyotropic liquid crystal phase is a rarely reported structure for lipopeptides;[21−24] to the best of our knowledge, nematic hydrogels have not been previously reported. We then investigate the organocatalytic activity of PAEPKI-C_{16} using a model aldol reaction of *p*-nitrobenzaldehyde and cyclohexanone, and the results are compared to those for C_{16}-IKPEAP previously reported elsewhere.[13]

In addition, the cytotoxicity and anticancer activity of PAEPKI-C_{16} are examined and compared to the corresponding measurements for C_{16}-IKPEAP. PYY_{3-36} is an agonist for the Y_2 receptor, which is a G-protein-coupled receptor. Y_2 receptors are known to play a role in tumor development and are recognized as tumor markers overexpressed on the surface of cancer cells.[25] Therefore, PYY_{3-36} derivatives may have potential in cancer therapeutics. In addition, proline metabolism plays a key role in cancer, with an important connection to genes regulating the p53 tumor suppressor protein,[26] and as such, this pathway has emerged as a potential cancer therapy target.[27] Conjugation of a free proline to a short lipidated peptide as in PAEPKI-C_{16} may provide a substrate with

https://dx.doi.org/10.1021/acsami.0c00686
ACS Appl. Mater. Interfaces XXXX, XXX, XXX−XXX

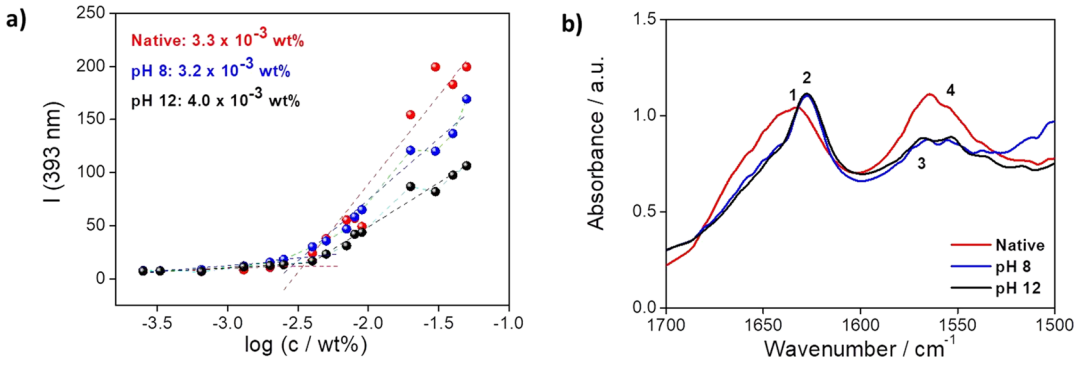

Figure 1. (a) Comparison of the concentration dependence of PAEPKI-C_{16} and the pyrene fluorescence I (393 nm). The inflection point of the curve intersection corresponds to the cac of each sample. (b) FTIR data of 2 wt % D_2O solutions of the peptide, considering different concentrations and pH.

anticancer activity, which is investigated herein in an initial study using breast cancer cells. Its cytotoxicity is compared to that against fibroblasts.

MATERIALS AND METHODS

Materials. PAEPKI-C_{16} (TFA salt) was synthesized by Peptide Synthetics, U.K. The molecular weight determined by mass spectrometry was 877.20 g mol^{-1} (expected: 877.2 g mol^{-1}), and the purity by HPLC was >95.0%. C_{16}-IKPEAP (ammonium acetate salt) was synthesized by Peptide Synthetics, U.K. The molecular weight determined by mass spectrometry was 892.18 g mol^{-1} (expected: 891.60 g mol^{-1}), and the purity by HPLC was >95.0%.

Fluorescence Spectroscopy. Fluorescence spectra were recorded as described previously.[28] ANS assays were performed using 3.25×10^{-4} to 0.13 wt % peptide in 2.1×10^{-3} wt % 8-anilino-1-napthalenesulfonic acid (ANS) solution. Pyrene assays were performed using 3.25×10^{-4} to 0.13 wt % peptide in 2.167×10^{-5} wt % pyrene solution.

Fourier-Transform Infrared Spectroscopy (FTIR). FTIR spectra were recorded as described previously.[28] Samples containing 1 and 2 wt % lipopeptides in D_2O at pH native, 8, and 12 were measured using CaF_2 plate windows with a 6 μm spacer. The spectra were scanned 118 times over the range of 4000 to 500 cm^{-1} and at a resolution of 4 cm^{-1}. An averaged D_2O spectrum was used as the background, and its signal was subtracted from the experimental data.

Circular Dichroism (CD). CD spectra were recorded as described previously.[29] Quartz plaques (0.1 and 0.01 mm thick) were used for the experiments at native pH, pH 8 and pH 12.

Ellipticity is reported as the mean residue ellipticity ($[\theta]$, in degrees cm^2 $dmol^{-1}$) and calculated as $[\theta] = [\theta]_{obs}$ MRW/10cl, where $[\theta]_{obs}$ is the ellipticity measured in millidegrees, MRW is the mean residue molecular weight of the peptide (molecular weight divided by the number of amino acid residues), c is the concentration of the sample in mg/mL, and l is the optical path length of the cell in centimeters.

Cryogenic Transmission Electron Microscopy (Cryo-TEM). Cryo-TEM images were obtained as described previously.[28]

Small-Angle X-ray Scattering (SAXS). SAXS experiments were performed on the bioSAXS beamline B21 at Diamond Light Source, U.K., as described previously.[28]

Aldol Reactions in Water. Cyclohexanone (0.9 mmol, 85 μL) was added to the peptide catalysts (3.3 μmol, 3.0 mg), varying the amount of water (170 μL, 85 μL, and in the absence). *p*-Nitrobenzaldehyde (67.9 μmol, 10.3 mg) was added, and the reaction mixture was stirred at room temperature for 3 days before being extracted with ethyl acetate four times. For the experiment containing no water, 0.5 mL of water was added to the system before extraction, to help in the phase separation. NMR measurements using a (^{1}H) Bruker Ultrashield 300 were performed at 300 MHz with a deuterated chloroform solvent. The yield and diastereomer *anti:syn* ratio were calculated using the NMR spectrum obtained, where tetramethylsilane (TMS) was used as a reference. ^{1}H NMR (300 MHz, $CDCl_3$): δ 8.22−8.18 (m, 2H, ArH); 7.51−7.47 (m, 2H, ArH); 5.47 (br s, 1H, C*H*OH-*syn*); 4.89 (dd, J = 7.5 Hz, 3.0 Hz, 1H, C*H*OH-*anti*); 4.08 (d, J = 3.0 Hz, 1H, CHO*H*-*anti*); 2.66−2.30 (m, 1H, C*H*CHOH); 2.66−2.30 (m, 2H, $CH_2C(O)$); 2.16−1.24 (m, 6H, chex-H).

Cytocompatibility Studies. In vitro cell culture was carried out using HCT-116 (ECAAC human colorectal tumor cell line) and HDFa (human dermal fibroblast cells). HCT-116 was cultured in McCoys 5A modified medium with 10% fetal bovine serum (FBS) and 1% antibiotic-antimycotic solution (ThermoScientific, 100×). HDFa cells were cultured in DMEM F12 media supplemented with 5% FBS, 1% antibiotic-antimycotic solution, and 100 μg/mL insulin. The cells were maintained in a humidified atmosphere of 5% CO_2 at 37 °C.

The effect of C_{16}-IKPEAP and PAEPKI-C_{16} on cell viability was assessed using an MTT (3-(4,5- dimethylthiazol-2-yl)-2,5-diphenyltetrazolium bromide) assay. The cells were seeded into a 96-well plate and incubated for 24 h, to allow the cells to adhere at a seeding density of either 1×10^4 or 4×10^4 cells/mL for HCT-116 and HDFa, respectively. After this, a total volume of 100 μL of the peptide dissolved in complete medium was added, to yield final peptide concentrations ranging from 0.06 to 4×10^{-4} wt %. Negative controls containing 100 μL of complete medium were also included. After 67 h of incubation, 20 μL of MTT (0.5 wt % in PBS) was added to each well plate and allowed to incubate for 5 h (total of 72 h incubation). After this, the solutions were removed from the wells and replaced with 100 μL of DMSO and incubated for 30 min. The absorbance was read using a microplate reader (λ = 570 nm). The absorbance readings were compared against the negative control to obtain % viability. Data are fitted with a sigmoidal line as a guide to the eye. Statistical tests, ANOVA, and Bonferroni correction, were used to assess significance.

Scanning Electron Microscopy (SEM). The 3 wt % pH 8 hydrogel was immersed in a fixative solution containing 2.5% glutaraldehyde for 60 min at 5 °C. This was followed by gradual dehydration from 10 to 100% ethanol (10, 30, 50, 70, 90, and 100% ethanol), with 30 s time intervals between each step. The sample was then extracted from the 100% ethanol solution and subjected to critical point drying. The dried material was placed on a stub covered with a carbon tab (Agar Scientific, U.K.), and then coated with gold. An FEI Quanta FEG 600 environmental scanning electron microscope (SEM) in high vacuum mode (20 kV high tension) was used to study and record SEM images.

Electrospinning. Electrospinning was performed using a syringe connected to a 25 kV voltage power supply (Glassman Inc.) and a syringe pump (Kd Scientific Model 200 Series). An aliquot of 1 mL of the 5 wt % hydrogel was used for electrospinning at a distance between the needle and collector of 10 cm in a 1 mL/h flow. One TEM grid was attached to the aluminum plate, and after drying at room temperature, TEM images were obtained as described above.

https://dx.doi.org/10.1021/acsami.0c00686
ACS Appl. Mater. Interfaces XXXX, XXX, XXX−XXX

RESULTS AND DISCUSSION

The critical aggregation concentration (cac) for the peptide PAEPKI-C_{16} at three different pH values (native, 8, and 12) was determined using a 2.2×10^{-5} wt % pyrene solution as the fluorescent probe. Considering the emission band located approximately at 393 nm and comparing these results as a function of the logarithm of the peptide concentration, it is possible to determine the cac by break points in the concentration dependent intensities (Figure 1 a). The fluorescence spectra can be seen in Figure S1. A similar cac was observed for the samples at native pH and pH 8, being $(3.3 \pm 0.2) \times 10^{-3}$ wt % and $(3.2 \pm 0.2) \times 10^{-3}$ wt %, respectively, suggesting that self-assembly occurs similarly for both systems. In basic conditions (pH 12), a slight enhancement of the cac to $(4.0 \pm 0.2) \times 10^{-3}$ wt % was observed, suggesting that hydrophobicity decreases as the pH is increased. For comparison, C_{16}-IKPEAP has a similar cac $(2.9 \pm 0.2) \times 10^{-3}$ wt % at native pH.[20]

In order to study the secondary structure under distinct environmental conditions, including peptide concentration, pH, and temperature variation, FTIR and CD experiments were performed. The results are shown, respectively, in Figures 1b and 2. The FTIR spectra in the amide I′ and II′ regions are presented in Figure 1b. For all samples, the characteristic bands are located at 1628−1636 cm^{-1} (peaks 1 and 2) and at 1553−1554 cm^{-1} (peaks 3 and 4). The former are assigned to β-sheet structure.[30−32] Considering the first set of peaks, the sample at native pH contains a peak at 1636 cm^{-1} (peak 1), whereas the other samples show peak 2 located at 1628 cm^{-1}. This effect suggests a higher β-sheet content for the pH 8 and pH 12 samples. The broad underlying peak shape, however, indicates an inhomogeneous ensemble with possible contributions from other structures such as poly(proline II).[33]

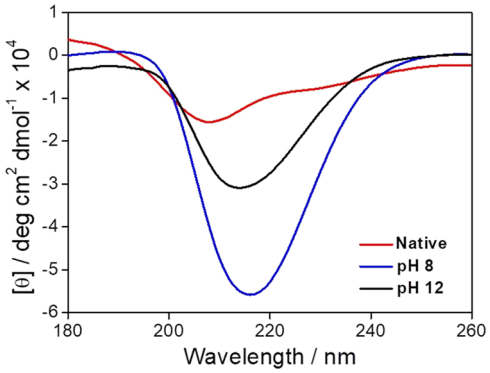

Figure 2. CD spectra for 0.04 wt % PAEPKI-C_{16} water solutions at the pH conditions shown.

Peaks 3 and 4 are in the range of the amide II band in H_2O; however, this is shifted to wavenumbers below 1500 cm^{-1} in D_2O.[34] Therefore, these peaks are assigned mainly to the side-chain asymmetric stretch vibrations of the COO^- groups in the E residues, which give a peak at 1567 cm^{-1} in D_2O.[31,32] A fraction of residual H_2O in the solutions may also lead to a component of amide II features.

Figure 2 shows the CD spectra of 0.04 wt % solutions at 20 °C, which show a minimum at 207, 213, and 216 nm, respectively, for native, pH 8, and pH 12, consistent with β-sheet structures.[35−37] The spectra do not contain the typical maximum observed just below 200 nm for typical β-sheet structures and in fact somewhat resemble the spectra observed for poly(L-proline) at high temperatures.[38] However, the presence of β-sheet structures is independently confirmed both by the FTIR spectra and the formation of fibril structures, as will be discussed shortly. Upon increasing the concentration of the peptide to 0.5 wt % at 20 °C, the location of the minima in the spectra shifted to 232, 229, and 226 nm (Figure S2). The red shift of the peak position may be due to increased twisting of the β-sheets, along with potential light scattering from the suspensions of highly extended fibers (vide infra).[39] Upon heating these systems from 20 to 80 °C, differences in the negative band intensity were seen (Figure S2). At native conditions, the increase of the temperature promoted a gradual enhancement of the minimum. The opposite effect occurred at pH 8, which showed a decrease in the minimum intensity with the increasing temperature. A very large minimum was observed for the sample at pH 12 at low temperatures, which is due to the formation of highly extended fibrils, as will be discussed shortly.

Cryo-TEM was used to image self-assembled structures, and the images can be seen in Figure 3. These show the formation of fibrils, with a population of oligomers at native pH. With the increase of pH, more fibers are observed. The fibrils extend to micrometers in length (Figure S3), especially at high pH. In addition, an increase in fiber thickness can be observed at high pH along with an increase in the alignment of the fibrils.

To further investigate the self-assembled fibril structure, SAXS was performed. The SAXS intensity profiles were fitted using the long cylinder shell form factor and Gaussian size distribution from the SASfit[40] package, producing fits shown as red lines in Figure 4a. Table S1 summarizes the fitted parameters. The length of the cylinders (L) was fixed at 1000

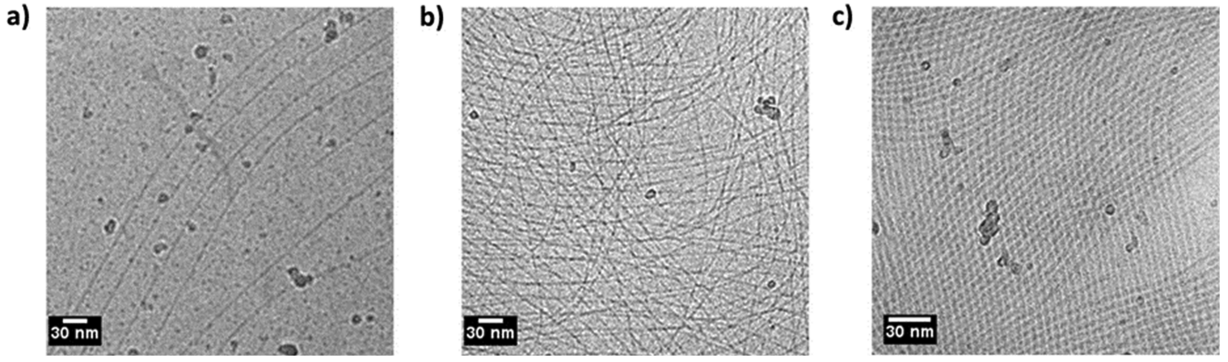

Figure 3. Cryo-TEM images of 1 wt % PAEPKI-C_{16} at (a) native, (b) pH 8, and (c) pH 12.

https://dx.doi.org/10.1021/acsami.0c00686
ACS Appl. Mater. Interfaces XXXX, XXX, XXX−XXX

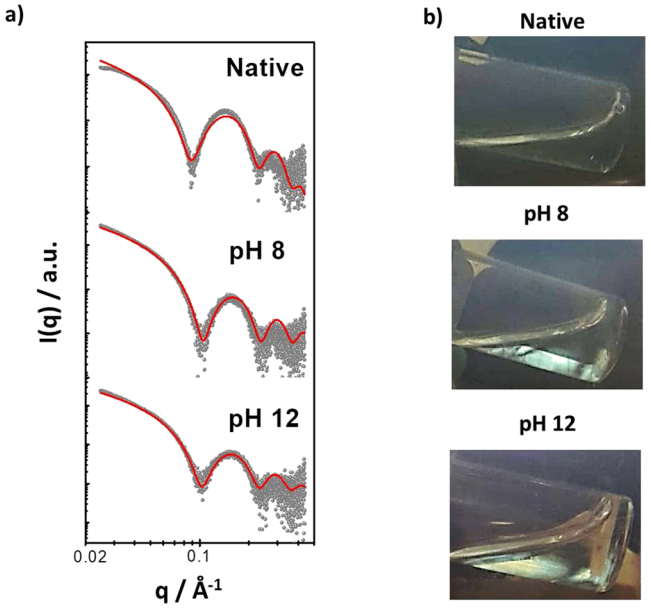

Figure 4. (a) SAXS data (gray symbols) and fitted form factors using a long cylindrical shell model (red lines) for 1 wt % PAEPKI-C_{16} water solutions, varying the pH. (b) Images of the birefringence of the samples in vials placed between crossed polarizers.

nm (with $L \gg R$, this parameter only represents a scaling parameter), and the scattering length density of the solvent (η_{solv}) was fixed. The cylinder radius (R) was 2.15 ± 0.2 nm, independent of pH. However, an increase of the shell thickness (ΔR) from 0.3 to 0.5 nm is observed with increasing pH (this corresponds to only the outer residues of the peptide, some of which are part of the "core"). In the low q vector region, the SAXS curves show differences for horizontal and vertical scattering, especially at high pH, as can be seen in Figure S4. This anisotropy in the low q SAXS patterns is due to the formation of spontaneously aligned nematic liquid crystal structures, as will be discussed shortly.

Another important effect monitored was the electron density distribution in the self-assembled structures. Considering the scattering length density of the core (η_{core}) and shell (η_{shell}), it was observed (Table S1) that the higher the pH, the higher is the core density and the lower is the shell density, pointing to the formation of more compact structures at high pH.

Since cryo-TEM shows the presence of aligned fibers and SAXS in 1 wt % aqueous solutions also indicates significant sample anisotropy, the macroscopic sample birefringence was examined for samples placed in glass flasks between crossed polarizers. An increase of the birefringence is observed with increasing pH, as shown in Figure 4b. In this case, the native system was the only system that did not present anisotropy.

We reasoned that since PAEPKI-C_{16} self-assembles into highly extended fibrils, it might be possible to form hydrogels at a sufficiently high concentration due to the formation of (noncovalently) cross-linked fibrillar networks. Upon increasing the peptide concentration to 5 wt %, only the pH 8 sample (Figure 5) spontaneously formed a soft hydrogel at room temperature. The other samples (native and pH 12) were subjected to a heating−cooling process, and after this, the pH 12 sample formed a hydrogel, while the native remained in solution, as can be seen in Figure 5. The tube inversion test shows the existence of (finite yield stress) hydrogels.

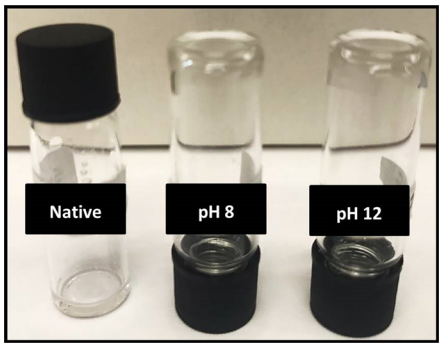

Figure 5. Images of 5 wt % PAEPKI-C_{16} solutions at native, pH 8, and pH 12.

The fibrillar structure of the hydrogels was confirmed through a combination of SEM, SAXS, and TEM, as shown in Figure 6. The SEM image in Figure 6a shows a fibrillar network structure. SAXS data from gels showed form factor features (Figure 6b), which could be fitted with the same cylindrical shell form factor model as for solutions, with a similar fibril core radius and shell thicknesses (Table S2). This shows that the hydrogels are formed from a network of ultrafine peptide fibrils, with a radius of approximately 2 nm. As for solutions, the PAEPKI-C_{16} hydrogels also showed birefringence, which was higher at pH 12, as can be seen in Figure 6c, which shows gels suspended in liquid. We also attempted to generate electrospun macroscopic fibers from concentrated solutions of the lipopeptide, and although this was not possible, we were able to image fibrils in the electrospun droplets using TEM (Figure 6d).

The importance of the availability of the proline residue in peptide sequences for aldol reactions has been highlighted.[3] Also, in comparison with the recently studied C_{16}-IKPEAP lipopeptide, we monitored the efficiency of PAEPKI-C_{16} as a catalyst in asymmetric aldol reactions using *p*-nitrobenzaldehyde, cyclohexanone, and water, presented in Scheme 2.

Table 1 summarizes the conversion and stereoselectivity of the aldol products, with comparison of both peptides. The NMR results for entries 1, 2, and 3 can be seen in Figure S5. For these reactions, 5 mol % catalyst solutions were used, with an excess of cyclohexanone (12 equiv), following the same experimental methodology for C_{16}-IKPEAP.[20] The assignment of the stereoisomers obtained was based on the literature.[41]

The influence of water on the catalyzed aldol reaction was evaluated, and entries 1−3 and 6 were stabilized in solution, while entries 4 and 5 form hydrogels during the reaction process. The best conditions presented for both peptides are described in entries 3 and 6, which presented high conversion (56 and 34% for PAEPKI-C_{16} and C_{16}-IKPEAP, respectively) and good diastereoselectivity (84:16 and 36:64). Based on this result, it was possible to conclude that the absence of water in the reaction medium favored the formation of the *anti*-aldol product, which can be related to the access of the reagents to the proline residues in the organic phase. PAEPKI-C_{16} shows enhanced diastereoselectivity compared to C_{16}-IKPEAP under all conditions examined and conversion under conditions except 1 equiv of H_2O, when it was slightly lower than for C_{16}-IKPEAP. These results show that the molecular structure of the peptide influences the conversion and diastereoselectivity of the reactions. Depending on the mode of self-assembly, the enamine transition state formed can favor the attack of the

https://dx.doi.org/10.1021/acsami.0c00686
ACS Appl. Mater. Interfaces XXXX, XXX, XXX−XXX

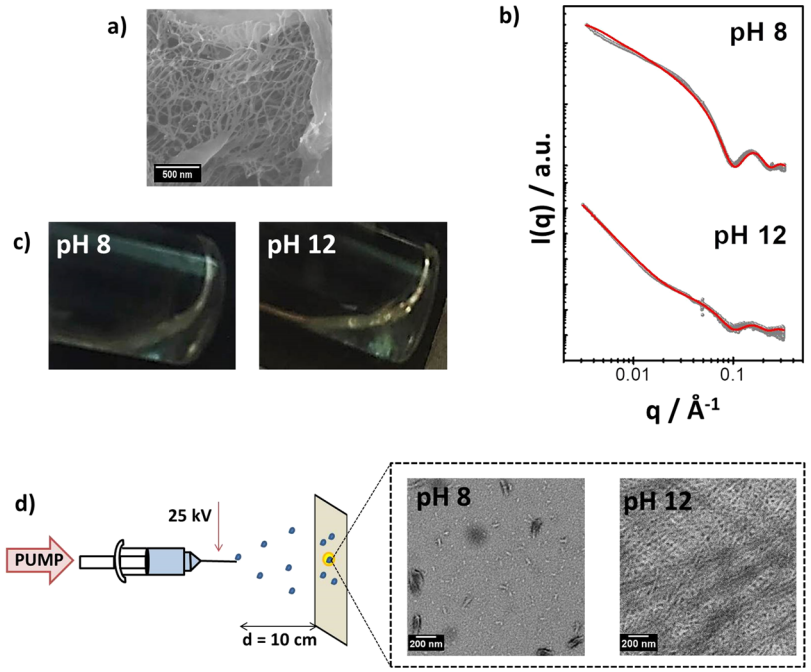

Figure 6. (a) SEM image showing fiber structures in a pH 8 hydrogel. (b) SAXS data (gray) and fitted form factor (red) using a cylindrical shell model for 3 wt % PAEPKI-C_{16} hydrogels, at two pH values indicated. (c) Images of the birefringence between crossed polarizers of the 3 wt % samples. (d) Scheme of the electrospinning procedure and TEM images of the electrospun 5 wt % gel samples.

Scheme 2. Aldol Reaction Mechanism Using *p*-Nitrobenzaldehyde and Cyclohexanone as Reagents, Catalyzed by PAEPKI-C_{16} at Native pH

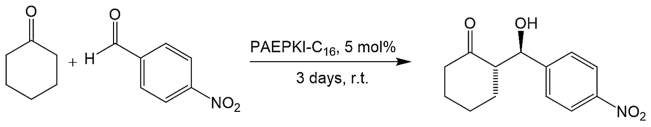

Table 1. Conversion and Diastereoselectivity of the Direct Aldol Reaction of *p*-Nitrobenzaldehyde and Cyclohexanone for PAEPKI-C_{16} Compared to the Peptide Derivative C_{16}-IKPEAP[20]

entry[a]	peptide	catalyst (mol %)	H_2O[b] (equiv)	conversion[c] (%)	*anti:syn*[c]
1	PAEPKI-C_{16}	5	2.0	7.9	78:22
2		5	1.0	8.7	81:19
3		5	0.0	56	84:16
4	C_{16}-IKPEAP	5	2.0	3.6	15:85
5		5	1.0	10	51:49
6		5	0.0	34	36:64

[a]The reactions were performed at room temperature with vigorous stirring for 72 h. [b]Water excess in relation to cyclohexanone (v/v). [c]Yield and diastereoselectivity were obtained by ^{1}H NMR analysis of the gross product.

ketone and aldehyde at the catalytic surface, i.e., the proline-functionalized surface of the self-assembled structures.

Cytocompatibility studies of C_{16}-IKPEAP and PAEPKI-C_{16} were performed using an MTT assay on human breast cancer (MCF-7) and human dermal fibroblast (HDFa) cells to determine cell viability (Figure 7) and to examine whether there was any selectivity toward cancer cells. HDFa was used as a control cell line in order to observe whether there is a preferential effect against the cancer cell line. The results are summarized in Table 2.

A difference is noted in the IC50 values for C_{16}-IKPEAP against MCF-7 and HDFa cells, corresponding to 0.021 wt % or 0.24 μM. However, PAEPKI-C_{16} exhibited a stronger activity against HDFa than MCF-7. Generally, PAEPKI-C_{16} is more toxic than C_{16}-IKPEAP, which is presumably due to the different modes of self-assembly. The peptide residues in PAEPKI-C_{16} are present at a high density on the surface of highly elongated fibers, whereas those in C_{16}-IKPEAP are present on the surface of micelles.

The difference in the catalytic behavior and cytotoxicity is influenced by the very different self-assembly properties of PAEPKI-C_{16} and C_{16}-IKPEAP. The enhanced catalytic activity is likely due to the high density of the free prolines present at the surface of the fibrils of PAEPKI-C_{16}. The higher cytotoxicity of this lipopeptide is also likely due to the formation of extended nanostructures. It is known for polymeric and inorganic nanoparticles, for example, that the shape of the nanostructure significantly influences cytotoxicity.[42−45] Among other effects, this can arise due to the different modes of internalization of anisotropic particles. In a series of papers, the Stupp group has highlighted that the presence of peptide motifs on the surface of fibrils formed by lipopeptides enhances bioactivity.[46−48] The highly distinct modes of self-assembly of the two lipopeptides studied here lead to significant differences in biocatalytic activity and cytotoxicity. At the molecular level, this must be due to the configuration of the peptide forming the surface corona of the nanostructures and the linker group. The electrostatic repulsion of the C-terminal P-COOH units in C_{16}-IKPEAP is likely to favor the formation of micelles, whereas this interaction is suppressed in PAEPKI-C_{16}, and stacking of the hydrophobic terminal P and A residues promotes β-sheet formation. This may also be favored by the salt bridging interactions between the E and K residues in PAEPKI-C_{16}, which are not hindered by the presence of the additional C-terminal charge in C_{16}-IKPEAP. It should be noted that the

https://dx.doi.org/10.1021/acsami.0c00686
ACS Appl. Mater. Interfaces XXXX, XXX, XXX−XXX

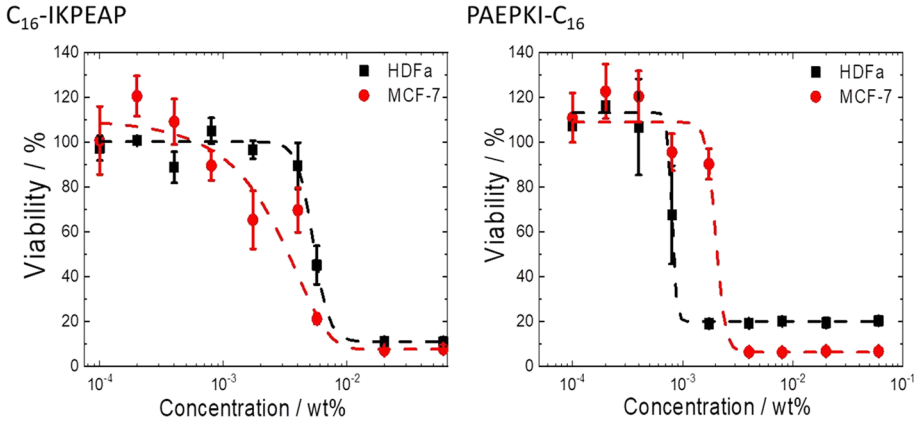

Figure 7. MTT assay of the viability of fibroblasts (HDFa) and breast cancer MCF-7 cells as a function of concentration of C_{16}-IKPEAP and PAEPKI-C_{16}.

Table 2. Cytocompatibility Results (IC_{50} Values) for C_{16}-IKPEAP and PAEPKI-C_{16}

	C_{16}-IKPEAP		PAEPKI-C_{16}	
cell line	wt %	μM	wt %	μM
HDFa	0.034	0.39	0.0084	0.10
MCF-7	0.055	0.63	0.0200	0.23

increase in the fibril alignment and nematic phase birefringence observed upon increasing pH is ascribed to the likely predominant effect of pH on the charge of the lysine residue, the side chain of which has a pK_a of 10.5, although this can be modified by the presence of other residues (for example, the nearby glutamic acid residue).[49,50] Proline also has a reported pK_a of the amine group near pK_a 11.[50] At high pH, the lysine and proline residues will be deprotonated, leading to a loss of the positive charges in the peptide, which may lead to increased electrostatic interactions between the anionic glutamic acid residues on peptides within the fibril, possibly causing an increased fibril persistence length.

CONCLUSIONS

Our study shows many significant differences in the self-assembly behavior and properties when comparing lipopeptide homologues with reversed sequence and lipid chain attachment. The results of PAEPKI-C_{16} presented here show that it forms highly elongated β-sheet fibril structures, especially at pH 8−12, in complete contrast to C_{16}-IKPEAP, which has previously been shown to form spherical micelles.[20] The critical aggregation concentrations for the two lipopeptides are similar; however, the aggregated structure is very distinct. The formation of a nematic phase is only possible with extended structures such as fibrils; therefore, it is not surprising that this is not observed for C_{16}-IKPEAP, which forms micellar aggregates. The ability of PAEPKI-C_{16} to form hydrogels (at sufficiently high pH) is also notable (and may be contrasted with C_{16}-IKPEAP). To the best of our knowledge, nematic hydrogels have not been previously reported for self-assembling lipopeptides, although they are known for amyloid-forming peptides.[51−53] It is evident that the gelation correlates with the formation of highly extended fibrils, the presence of which within the hydrogels is confirmed by in situ SAXS. The fibril network is based on ultrafine fibers with a core radius of only 2 nm.

The catalytic activity of the two lipopeptides is also quite different, as demonstrated by our model aldol reaction analysis. PAEPKI-C_{16} shows a significant enhancement in diastereoselectivity compared to C_{16}-IKPEAP under the same reaction conditions. The conversion is also significantly higher for PAEPKI-C_{16} under most conditions (with one exception, Table 1). This is ascribed to the presence of a free proline residue in PAEPKI-C_{16} in contrast to C_{16}-IKPEAP with C-terminal amide-linked proline.

Remarkable significant differences in the cytotoxicity of PAEPKI-C_{16} and C_{16}-IKPEAP were observed, the former being substantially more cytotoxic (lower IC50) against both fibroblast and MCF-7 breast cancer cell lines. This peptide shows preferential activity against fibroblasts rather than MCF-7 cells, in contrast to C_{16}-IKPEAP, which has a lower IC50 against the cancer cell line compared to HDFa fibroblasts.

The formation of birefringent nematic structures in dilute aqueous solution is a notable feature of PAEPKI-C_{16} self-assembly. These lyotropic liquid crystal structures may be of future use, for example, in the measurement of residual dipolar couplings, which facilitates assignments in solution NMR of biomacromolecules, as recently demonstrated,[54] for example, for the nematic phase of an amyloid peptide in methanol.[55] A water-based system such as PAEPKI-C_{16} may be highly beneficial for this and applications such as tissue engineering or responsive sensing.

ASSOCIATED CONTENT

Supporting Information

The Supporting Information is available free of charge at https://pubs.acs.org/doi/10.1021/acsami.0c00686.

Fluorescence emission and CD spectra, additional cryo-TEM images, analysis of SAXS pattern anisotropy and SAXS fitting parameter, and NMR spectra for the aldol reaction analysis (PDF)

AUTHOR INFORMATION

Corresponding Author

Ian W. Hamley − *Department of Chemistry, University of Reading, Reading RG6 6AD, U.K.;* orcid.org/0000-0002-4549-0926; Email: I.W.Hamley@reading.ac.uk

Authors

Juliane N.B.D. Pelin − *Department of Chemistry, University of Reading, Reading RG6 6AD, U.K.; Centro de Ciências Naturais*

https://dx.doi.org/10.1021/acsami.0c00686
ACS Appl. Mater. Interfaces XXXX, XXX, XXX−XXX

e Humanas, Universidade Federal do ABC, Santo André 09210-580, Brazil

Charlotte J. C. Edwards-Gayle − *Department of Chemistry, University of Reading, Reading RG6 6AD, U.K.*

Valeria Castelletto − *Department of Chemistry, University of Reading, Reading RG6 6AD, U.K.;* orcid.org/0000-0002-3705-0162

Andrea M. Aguilar − *Instituto de Ciências Ambientais, Químicas e Farmacêuticas, Universidade Federal de São Paulo, Diadema 09972-270, Brazil*

Wendel A. Alves − *Centro de Ciências Naturais e Humanas, Universidade Federal do ABC, Santo André 09210-580, Brazil;* orcid.org/0000-0002-8394-2751

Jani Seitsonen − *Nanomicroscopy Center, Aalto University, FIN-02150 Espoo, Finland*

Janne Ruokolainen − *Nanomicroscopy Center, Aalto University, FIN-02150 Espoo, Finland*

Complete contact information is available at: https://pubs.acs.org/10.1021/acsami.0c00686

Notes

The authors declare no competing financial interest.

■ ACKNOWLEDGMENTS

This work was supported by EPSRC grant EP/L020599/1 to IWH. JNBDP acknowledges FAPESP (project number 2015/20446-9 and 2018/12535-0) for a doctoral fellowship and the research internship abroad program (BEPE). WAA acknowledges the São Paulo Research Foundation (FAPESP grant no. 2017/02317-2). CJCEG was supported by a studentship cofunded by the University of Reading and Diamond Light Source. We thank Jessica Hutchinson for preliminary studies. We are grateful to Diamond for the award of beamtime on beamline B21 (SM21470-2 and SM22925-1), and especially Nathan Cowieson for help during the experiments. The authors acknowledge access to the Chemical Analysis Facility at University of Reading, and Saaed Mohan for assistance with the electrospinning experiments.

■ REFERENCES

(1) Hernández, J. G.; Juaristi, E. Recent Efforts Directed to the Development Of More Sustainable Asymmetric Organocatalysis. *Chem. Commun.* **2012**, *48*, 5396−5409.

(2) Zhong, L.; Gao, Q.; Gao, J.; Xiao, J.; Li, C. Direct Catalytic Asymmetric Aldol Reactions on Chiral Catalysts Assembled in the Interface of Emulsion Droplets. *J. Catal.* **2007**, *250*, 360−364.

(3) Soares, B. M.; Aguilar, A. M.; Silva, E. R.; Coutinho-Neto, M. D.; Hamley, I. W.; Reza, M.; Ruokolainen, J.; Alves, W. A. Chiral Organocatalysts Based on Lipopeptide Micelles for Aldol Reactions in Water. *Phys. Chem. Chem. Phys.* **2017**, *19*, 1181−1189.

(4) Rodríguez-Llansola, F.; Escuder, B.; Miravet, J. F. Switchable Performance of an L-Proline-Derived Basic Catalyst Controlled by Supramolecular Gelation. *J. Am. Chem. Soc.* **2009**, *131*, 11478−11484.

(5) Rodríguez-Llansola, F.; Miravet, J. F.; Escuder, B. A Supramolecular Hydrogel as a Reusable Heterogeneous Catalyst for the Direct Aldol Reaction. *Chem. Comm.* **2009**, *47*, 7303−7305.

(6) Mahrwald, R., Ed.; *Modern Aldol Reactions*; Wiley-VCH: Weinheim, 2004.

(7) List, B.; Lerner, R. A.; Barbas, C. F. Proline-Catalyzed Direct Asymmetric Aldol Reactions. *J. Am. Chem. Soc.* **2000**, *122*, 2395−2396.

(8) Pidathala, C.; Hoang, L.; Vignola, N.; List, B. Direct Catalytic Asymmetric Enolexo Aldolizations. *Angew. Chem., Int. Ed. Engl.* **2003**, *42*, 2785−2788.

(9) Löwik, D. W. P. M.; van Hest, J. C. M. Peptide Based Amphiphiles. *Chem. Soc. Rev.* **2004**, *33*, 234−245.

(10) Hamley, I. W. Self-Assembly of Amphiphilic Peptides. *Soft Matter* **2011**, *7*, 4122−4138.

(11) Matson, J. B.; Zha, R. H.; Stupp, S. I. Peptide Self-assembly for Crafting Functional Biological Materials. *Curr. Opin. Solid State Mat. Sci.* **2011**, *15*, 225−235.

(12) Hamley, I. W. Lipopeptides: from Self-assembly to Bioactivity. *Chem. Commun.* **2015**, *51*, 8574−8583.

(13) Castelletto, V.; Edwards-Gayle, C. J. C.; Hamley, I. W.; Pelin, J. N. B. D.; Alves, W. A.; Aguilar, A. M.; Seitsonen, J.; Ruokolainen, J. Self-Assembly of a Catalytically Active Lipopeptide and its Incorporation into Cubosomes. *ACS Appl. Bio Mater.* **2019**, *2*, 3639−3647.

(14) Coll, A. P.; Farooqi, I. S.; O'Rahilly, S. The Hormonal Control of Food Intake. *Cell* **2007**, *129*, 251−262.

(15) Tatemoto, K. Isolation And Characterization Of Peptide YY (PYY), a Candidate Gut Hormone that Inhibits Pancreatic Exocrine Secretion. *Proc. Natl. Acad. Sci. U. S. A.* **1982**, *79*, 2514−2518.

(16) Batterham, R. L.; Cowley, M. A.; Small, C. J.; Herzog, H.; Cohen, M. A.; Dakin, C. L.; Wren, A. M.; Brynes, A. E.; Low, M. J.; Ghatei, M. A.; Cone, R. D.; Bloom, S. R. Gut Hormone PYY_{3-36} Physiologically Inhibits Food Intake. *Nature* **2002**, *418*, 650−654.

(17) Boggiano, M. M.; Chandler, P. C.; Oswald, K. D.; Rodgers, R. J.; Blundell, J. E.; Ishii, Y.; Beattie, A. H.; Holch, P.; Allison, D. B.; Schindler, M.; Arndt, K.; Rudolf, K.; Mark, M.; Schoelch, C.; Joost, H. G.; Klaus, S.; Thöne−Reineke, C.; Benoit, S. C.; Seeley, R. J.; Beck-Sickinger, A. G.; Koglin, N.; Raun, K.; Madsen, K.; Wulff, B. S.; Stidsen, C. E.; Birringer, M.; Kreuzer, O. J.; Deng, X. Y.; Whitcomb, D. C.; Halem, H.; Taylor, J.; Dong, J.; Datta, R.; Culler, M.; Ortmann, S.; Castañeda, T. R.; Tschöp, M. PYY_{3-36} as an Anti-obesity Drug Target. *Obes. Rev.* **2005**, *6*, 307−322.

(18) Hutchinson, J. A.; Burholt, S.; Hamley, I. W.; Lundback, A.-K.; Uddin, S.; dos Santos, A. G.; Reza, M.; Seitsonen, J.; Ruokolainen, J. The Effect of Lipidation on the Self-Assembly of the Gut Derived Peptide Hormone PYY3-36. *Bioconjugate Chem.* **2018**, *29*, 2296−2308.

(19) Castelletto, V.; Hamley, I. W.; Seitsonen, J.; Ruokolainen, J.; Harris, G.; Bellmann-Sickert, K.; Beck-Sickinger, A. G. Conformation and Aggregation of Selectively PEGylated and Lipidated Gastric Peptide Hormone Human PYY_{3-36}. *Biomacromolecules* **2018**, *19*, 4320−4332.

(20) Hutchinson, J. A.; Hamley, I. W.; Torras, J.; Aleman, C.; Seitsonen, J.; Ruokolainen, J. Self-Assembly of Lipopeptides Containing Short Peptide Fragments Derived from the Gastrointestinal Hormone PYY_{3-36}: From Micelles to Amyloid Fibrils. *J. Phys. Chem. B* **2019**, *123*, 614−621.

(21) Hamley, I. W. Liquid Crystal Phase Formation by Biopolymers. *Soft Matter* **2010**, *6*, 1863−1871.

(22) Zhang, S.; Greenfield, M. A.; Mata, A.; Palmer, L. C.; Bitton, R.; Mantei, J. R.; Aparicio, C.; de la Cruz, M. O.; Stupp, S. I. A Self-Assembly Pathway to Aligned Monodomain Gels. *Nat. Mater.* **2010**, *9*, 594−601.

(23) Hamley, I. W.; Dehsorkhi, A.; Castelletto, V.; Furzeland, S.; Atkins, D.; Seitsonen, J.; Ruokolainen, J. Reversible Helical Ribbon Unwinding Transition of a Self-assembling Peptide Amphiphile. *Soft Matter* **2013**, *9*, 9290−9293.

(24) Castelletto, V.; Edwards-Gayle, C. J. C.; Greco, F.; Hamley, I. W.; Seitsonen, J.; Ruokolainen, J. Self-Assembly, Tunable Hydrogel Properties, and Selective Anti-Cancer Activity of a Carnosine-Derived Lipidated Peptide. *ACS Appl Mater. Interfaces* **2019**, *11*, 33573−33580.

(25) Mörl, K.; Beck-Sickinger, A. G. Modulation of Internalization by Ligand Modification. In *Trafficking of GPCRs*; Wu, G., Ed.; Elsevier: Amsterdam, 2015, Vol. *132*, pp 73−96.

(26) Phang, J. M.; Liu, W. Proline Metabolism and Cancer. *Front. Biosci.* **2012**, *17*, 1835−1845.

(27) Tanner, J. J.; Fendt, S. M.; Becker, D. F. The Proline Cycle As a Potential Cancer Therapy Target. *Biochemistry* **2018**, *57*, 3433−3444.

(28) Castelletto, V.; Edwards-Gayle, C. J. C.; Hamley, I. W.; Barrett, G.; Seitsonen, J.; Ruokolainen, J. Peptide-Stabilized Emulsions and Gels from an Arginine-Rich Surfactant-like Peptide with Antimicrobial Activity. *ACS Appl. Mater. Interfaces* **2019**, *11*, 9893−9903.
(29) Castelletto, V.; Kaur, A.; Kowalczyk, R. M.; Hamley, I. W.; Reza, M.; Ruokolainen, J. Supramolecular Hydrogel Formation in a Series of Self-Assembling Lipopeptides with Varying Lipid Chain Length. *Biomacromolecules* **2017**, *18*, 2013−2023.
(30) Stuart, B. *Biological Applications of Infrared Spectroscopy*; Wiley: Chichester, 1997.
(31) Barth, A. Infrared Spectroscopy of Proteins. *Biochim. Biophys. Acta-Bioenerg.* **2007**, *1767*, 1073−1101.
(32) Barth, A.; Zscherp, C. What Vibrations Tell us About Proteins. *Quater. Rev. Biophys.* **2002**, *35*, 369−430.
(33) Schweitzer-Stenner, R.; Eker, F.; Perez, A.; Griebenow, K.; Cao, X.; Nafie, L. A. The Structure of Tri-Proline In Water Probed by Polarized Raman, Fourier Transform Infrared, Vibrational Circular Dichroism, and Electric Ultraviolet Circular Dichroism Spectroscopy. *Biopolymers* **2003**, *71*, 558−568.
(34) Fabian, H.; Mäntele, W. Infrared Spectroscopy of Proteins. In *Handbook of Vibrational Spectroscopy*; Wiley online library, 2006. https://onlinelibrary.wiley.com/doi/pdf/10.1002/0470027320.s8201.
(35) Bulheller, B. M.; Rodger, A.; Hirst, J. D. Circular and Linear Dichroism of Proteins. *Phys. Chem. Chem. Phys.* **2007**, *9*, 2020−2035.
(36) Nordén, B.; Rodger, A.; Dafforn, T. R. *Linear Dichroism and Circular Dichroism: A Textbook on Polarized-Light Spectroscopy*; Royal Society of Chemistry: Cambridge, 2010.
(37) Woody, R. W. Circular Dichroism of Peptides and Proteins. In *Circular Dichroism. Principles and Applications*; Nakanishi, K.; Berova, N.; Woody, R. W., Eds.; Wiley-VCH: New York, 1994; pp 473−496.
(38) Tooke, L.; Duitch, L.; Measey, T. J.; Schweitzer-Stenner, R. Kinetics of the Self-Aggregation and Film Formation of Poly-L-Proline at High Temperatures Explored by Circular Dichroism Spectroscopy. *Biopolymers* **2010**, *93*, 451−457.
(39) Hamley, I. W.; Nutt, D. R.; Brown, G. D.; Miravet, J. F.; Escuder, B.; Rodríguez-Llansola, F. Influence of the Solvent on the Self-Assembly of a Modified Amyloid Beta Peptide Fragment. II. NMR and Computer Simulation Investigation. *J. Phys. Chem. B* **2010**, *114*, 940−951.
(40) Bressler, I.; Kohlbrecher, J.; Thünemann, A. F. SASfit: A Tool for Small-Angle Scattering Data Analysis Using a Library of Analytical Expressions. *J. Appl. Crystallogr.* **2015**, *48*, 1587−1598.
(41) Mase, N.; Nakai, Y.; Ohara, N.; Yoda, H.; Takabe, K.; Tanaka, F.; Barbas, C. F. Organocatalytic Direct Asymmetric Aldol Reactions in Water. *J. Am. Chem. Soc.* **2006**, *128*, 734−735.
(42) Champion, J. A.; Mitragotri, S. Role of Target Geometry in Phagocytosis. *Proc. Natl. Acad. Sci. U. S. A.* **2006**, *103*, 4930−4934.
(43) Christian, D. A.; Cai, S.; Garbuzenko, O. B.; Harada, T.; Zajac, A. L.; Minko, T.; Discher, D. E. Flexible Filaments for in Vivo Imaging and Delivery: Persistent Circulation of Filomicelles Opens the Dosage Window for Sustained Tumor Shrinkage. *Molec. Pharm.* **2009**, *6*, 1343−1352.
(44) Venkataraman, S.; Hedrick, J. L.; Ong, Z. Y.; Yang, C.; Ee, P. L. R.; Hammond, P. T.; Yang, Y. Y. The Effects of Polymeric Nanostructure Shape on Drug Delivery. *Adv. Drug Del. Rev.* **2011**, *63*, 1228−1246.
(45) Gratton, S. E. A.; Ropp, P. A.; Pohlhaus, P. D.; Luft, J. C.; Madden, V. J.; Napier, M. E.; DeSimone, J. M. The Effect of Particle Design on Cellular Internalization Pathways. *Proc. Natl. Acad. Sci. U. S. A.* **2008**, *105*, 11613−11618.
(46) Cui, H.; Webber, M. J.; Stupp, S. I. Self-Assembly of Peptide Amphiphiles: From Molecules to Nanostructures to Biomaterials. *Biopolymers* **2010**, *94*, 1−18.
(47) Moyer, T. J.; Kassam, H. A.; Bahnson, E. S. M.; Morgan, C. E.; Tantakitti, F.; Chew, T. L.; Kibbe, M. R.; Stupp, S. I. Shape-Dependent Targeting of Injured Blood Vessels by Peptide Amphiphile Supramolecular Nanostructures. *Small* **2015**, *11*, 2750−2755.
(48) Hendricks, M. P.; Sato, K.; Palmer, L. C.; Stupp, S. I. Supramolecular Assembly of Peptide Amphiphiles. *Acc. Chem. Res.* **2017**, *50*, 2440−2448.
(49) Hamley, I. W. *Introduction to Peptide Science*; in press ed; Wiley: Chichester, 2020.
(50) Voet, D.; Voet, J. G. *Biochemistry*; John Wiley: New York, 1995.
(51) Aggeli, A.; Nyrkova, I. A.; Bell, M.; Harding, R.; Carrick, L.; McLeish, T. C. B.; Semenov, A. N.; Boden, N. Hierarchical Self-Assembly of Chiral Rod-Like Molecules as a Model for Peptide β-sheet tapes, ribbons, fibrils and fibres. *Proc. Natl. Acad. Sci. U. S. A.* **2001**, *98*, 11857−11862.
(52) Aggeli, A.; Bell, M.; Boden, N.; Carrick, L. M.; Strong, A. E. Self-assembling Peptide Polyelectrolyte β-sheet Complexes Form Nematic Hydrogels. *Angew. Chem., Int. Ed. Engl.* **2003**, *42*, 5603−5606.
(53) Bolisetty, S.; Harnau, L.; Jung, J. M.; Mezzenga, R. Gelation, Phase Behavior, and Dynamics of beta-Lactoglobulin Amyloid Fibrils at Varying Concentrations and Ionic Strengths. *Biomacromolecules* **2012**, *13*, 3241−3252.
(54) Lei, X.; Qiu, F.; Sun, H.; Bai, L.; Wang, W.-X.; Xiang, W.; Xiao, H. A Self-Assembled Oligopeptide as a Versatile NMR Alignment Medium for the Measurement of Residual Dipolar Couplings in Methanol. *Angew. Chem., Int. Ed. Engl.* **2017**, *56*, 12857−12861.
(55) Krysmann, M. J.; Castelletto, V.; McKendrick, J. E.; Clifton, L. A.; Hamley, I. W.; Stain, C.; Harris, P. J.; King, S. M. Self-Assembly of Peptide Nanotubes in an Organic Solvent. *Langmuir* **2008**, *24*, 8158−8162.

https://dx.doi.org/10.1021/acsami.0c00686
ACS Appl. Mater. Interfaces XXXX, XXX, XXX−XXX